Eidgenössische Technische Hochschule Zürich
Swiss Federal Institute of Technology Zurich

Optical phase stabilization within a selective fiber network

Semester Thesis

Kaizhao Wang

July, 2022

Advisors: Roland Matt Dr. Jeremy Flannery Prof. Jonathan Home

Department of Physics, ETH Zürich

Contents

Chapter 1

Introduction

Atoms and ions are perfect candidates for quantum information processing, because they are naturally identical and usually have long coherence time. However, laser addressing is typically required to manipulate these qubits[3], which increase the complexity of these atom or ion based systems. Therefore, to eventually perform useful quantum information processing which demands high-fidelity operations and large number of qubits, it is crucial to have a stable and scalable optical addressing system. This thesis is accordingly divided into two sections. In the first part, the main goal is to achieve relative phase stability between different addressing channels, while in the second section, the design of a scalable addressing system is discussed.

1.1 Relative phase stabilization

It is important to stabilize the relative phase between different addressing channels to perform coherent operations on multi-qubit registers, e.g. deep circuit and coherent cross-talk cancellation. We here consider an optical network where light from one laser is split into multiple branches which are controlled with individual fiber-coupled acoustic-optic modulator (AOM). By increasing the proportion of co-propagating beam path and using fiber based well-shielded system, the relative phase can be considered rather stable when simply turn on different channels symmetrically. However, we notice a rapid relative phase drift while operating different channel in an asymmetric way, e.g turning on one of the AOM without running the other or driving them with different power.

The relative phase drift could be detrimental while implementing deep quantum circuits with uneven duty cycle on different qubits or applying coherent cross-talk compensation with imbalanced beams power, which effectively introduce anomalous z-rotations on different qubits.[6]

In this thesis, we investigate the source of the relative phase drifts and demonstrate a mitigation method. We find that it mainly origins from the heating effect of the injected RF power to the fiber-attached acoustic optical modulator (f-AOM) and manage to suppress the phase drift to below one degree per second.

1.2 Scalable addressing system

The laser addressing system can be abstractly seen as a black box taking one input beam and output M beams targeting M of the N qubits, where N is the total number of qubits and $M \leq N$. Apparently, one can generate N fixed beams targeting all the qubits and achieve the required function by turning off the $(N - M)$ unwanted beams. However, this method leads to a considerable waste of laser power when $M \ll N$, as the power has been divided evenly into all the N channels. Therefore, a selective addressing system is favorable in this case. Assuming that the N-beam system and the selective system have efficiency η_N and η_{sel} respectively, we would be able to increase the power on each channel by a factor of $\frac{\eta_{sel}}{\eta_N}\frac{N}{M}$ by changing to the selective system.

As for the design of such an addressing system, here we mainly take into account three main features which are vital to the performance, i.e. flexibility, speed, and scalability.

Flexibility Here, flexibility means the capability our system can be used to different M. For instance, in a trapped-ions system we could have following circumstances.

$M = 2$: Implementing one two-qubit gate.

$M = 4, 5, 6$: Implementing one two-qubit gate with cross-talk compensation on the neighboring ions.

$M = N$: Implementing global single qubit rotations.

Therefore, it would be favorable if our system can be adapted to different numbers of M without changing the overall architecture.

Speed Here, speed means the switching time from one set of target qubits to another. One of the most important reason of increasing the laser power is to achieve faster gate operations. Hence, it would make no sense if the switching time is comparable or even longer than the gain in the gate time.

scalability Here, systems with higher scalability are those easier to be enlarged while N increases.

In this thesis, our design is based on these three features. A detailed design and relevant considerations are given in the later part of the second chapter.

Chapter 2

Relative phase stabilization

In this chapter, we will first discuss the experimental setup used to measure the relative phase between two channels and nail down the origin of the phase drift we observe. Then, we will demonstrate a method to mitigate the phase drift and show the experimental results we have achieved with this method.

2.1 Experimental setup

All the measurement and experiment shown in this thesis is based on the LogiQ setup in the Trapped Ion Quantum Information group (TIQI) at ETH Zürich. In this experiment, the $S_{1/2}$ and $D_{5/2}$ levels in $^{40}Ca^{+}$ ions are used to encode the qubits. Therefore, 729 nm light corresponding to the transition frequency of these two levels are used to manipulate the qubits. As shown in Fig. 2.1, the locked narrow-linewidth 729 nm light is split by an 50:50 fiber splitter and fed to two f-AOMs (Gooch & Housego SFO5388-T-0.5C2W-3-F2S-01) respectively for individual control. The two beams are then fed into the Cryostat and focused to the ions. Here we mainly focus on the relative phase stability for the part shown in Fig. 2.1. The stability of the relative phase downstream in the Cryostat are still to be measured directly with ions. However, given prior experience that the phase drift at the ions and which measured in the setup shown in this thesis are at the same order, we believe that the phase drift at the f-AOM is at least one of the dominant sources if not the only one.

As shown in Fig. 2.2, to measure the relative phase between the two optical channels, we pickup 1% of the optical signal with a 99:1 fiber beam spiltter and recombine the two pickup beams. The interference optical beatnote is then transferred to electrical signal with a photodiode. To rule out the effect of the relative phase drift between the two control RF signals generated with two Direct Digital Synthesizer (DDS) channels[5], we also mix up the

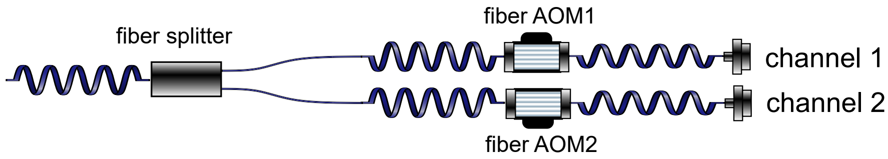

Figure 2.1: Schematic drawing of the addressing system being used. The 729 nm laser is split into two channels by a fiber splitter and individually controlled by fiber attached AOMs.

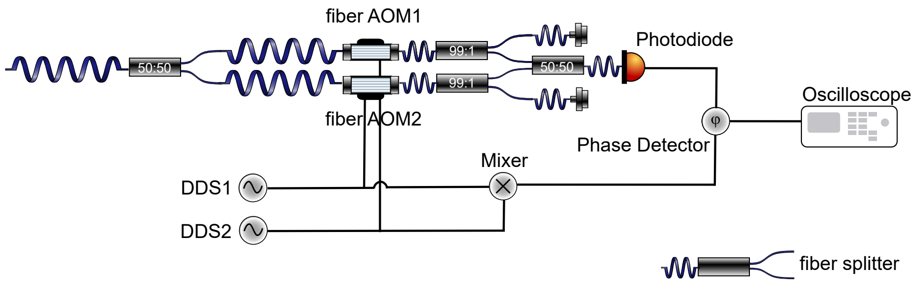

Figure 2.2: Schematic drawing of the experimental setup. The two beams are combined by a 50:50 beam splitter and detected by a photodiode. The optical beatnote is further compared with the RF beatnote using a phase detector to obtain the pure optical relative phase.

two RF signals with a RF Mixer (Mini-Circuits ZRPD-1+) and extract the pure optical phase difference by detect the phase difference between the RF beatnote and optical beatnote with a phase detector. The phase difference is then transferred into a DC voltage which can be easily read out with an oscilloscope.

2.1.1 General experiment procedure

To detect the phase with the setup shown in Fig. 2.2, the RF signals applied to the two channels need to have a frequency difference in order to generate the optical and RF beatnote. Given the center frequency of the f-AOMs at around 150 MHz, we set the RF frequency of DDS1, f_1, at 150 MHz and which on DDS2, f_2, at 152 MHz. In all the experiments shown below, test

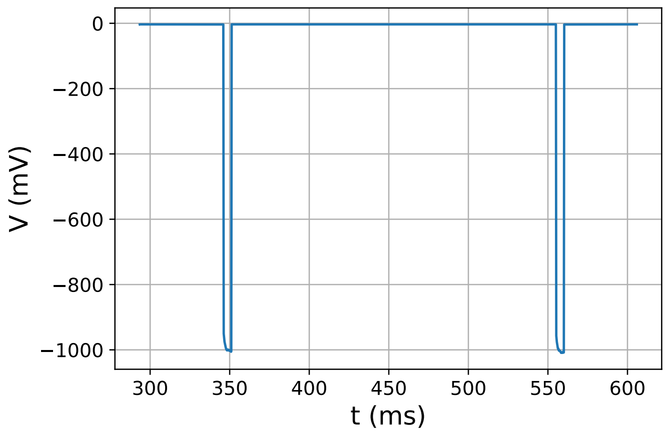

Figure 2.3: A test sequence between two detection pulses.

pulse sequences are interleaved with the detection pulses, i.e. setting $f_1 = 150\,\mathrm{MHz}$ and $f_2 = 152\,\mathrm{MHz}$ for a few milliseconds to extract the phase information. For instance, as shown in Fig. 2.3, a typical waveform seen on the oscilloscope would be periods of 0 V where the test pulse sequence is performed interleaved with pulses of positive or negative voltage signals which reveals the phase information.[1]

The phase detector is first calibrated, and we find that 10 mV approximately corresponds to 1 degree. We can then take the average value of the voltage within each detection pulse to approximate the relative optical phase at the center of pulse. Therefore, we can obtain the phase drift while repeating different test pulse sequences.

2.2 Phase drift and its origin

We first run a single pulse of 100 ms on channel 1 (Ch1) and channel 2 (Ch2) respectively. Later on, we run a combined pulse sequence with a 100ms pulse on Ch1 followed by the same pulse on Ch2. As shown in Fig. 2.4, when we only run pulses on one of the channels there is a rapid phase drift. However, when the pulses are run on both channels the phase drift is significantly suppressed. Therefore, we believe that the phase drift is due to the heating effect of the f-AOM while running pulses. However, there are two potential sources of heating, the injected optical power and RF power. In our case, the optical power is at the level of dozens of milliWatt while the RF power is at Watt level. Hence, we would expect the RF signal dominant the effect.

[1]Due to the setup of our control system, there is an approximately 450 μs idle time after each detection pulse.

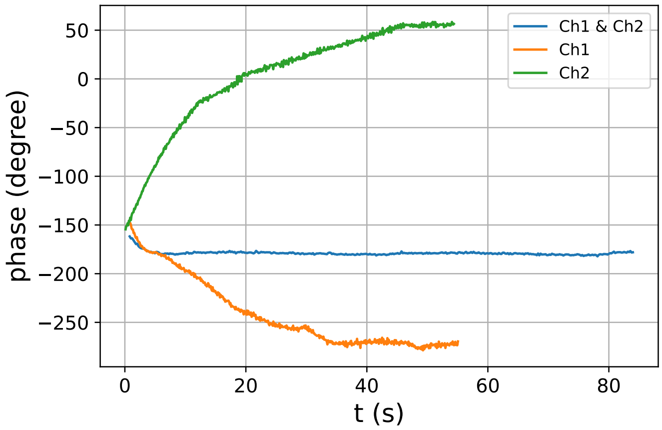

Figure 2.4: The three curves correspond to three test pulse sequences, i.e. a 100 ms pulse on Ch1, a 100ms pulse on Ch2 and, a 100 ms pulse on Ch1 followed by a 100 ms pulse on Ch2.

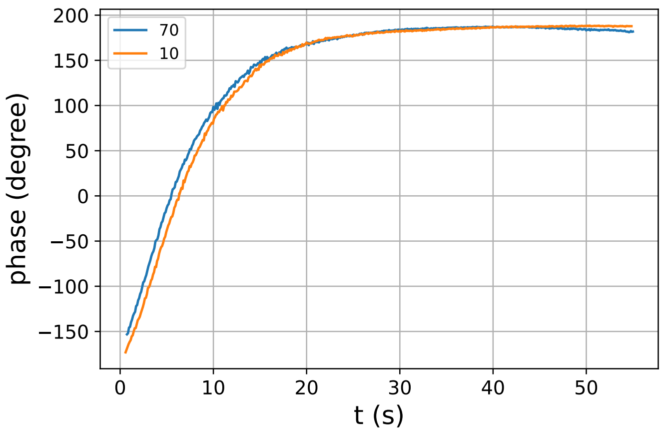

Figure 2.5: Here we use a 100ms pulse on Ch2 as our test sequence. We set the optical power by the double-pass AOM upstream to 10% and 70%.

This assumption is verified by measuring the phase drift at different RF power and optical power. We first keep the RF power as a constant and change the injected optical power controlled by a double-pass AOM upstream. As shown in Fig. 2.5, the slope of the curve looks rather similar even when the optical power is reduced to 10%.[2]

Then, we change the RF power applied to the f-AOM. Although the absorbed optical power would also be changed accordingly, as we have checked that the influence of the optical power is minor, we can still easily see the

[2]Here, the percentage power is the number used in Ionizer, the controlling interface used in TIQI group, which approximately follows a linear relationship with the actual power. However, a slight discrepancy is also observed.

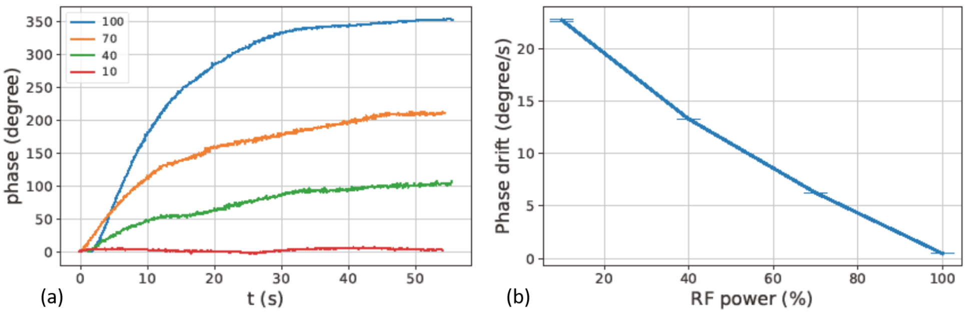

Figure 2.6: Here we use a 100ms pulse on Ch2 as our test sequence. We set the RF power applied on the f-AOMs to 10%, 40%, 70% and 100%.

dominant effect. As shown in Fig. 2.6, the lower the RF power applied to the f-AOM the slower the phase drift is. As shown in Fig. 2.6 (b), the speed of the phase drift and the RF power approximately follow a linear relationship[3]. From the above two experiments, we conclude that the dominant source of heating which causes the relative phase drift is the RF power injected into the f-AOM. However, here we are not sure the specific source of thermal expansion leading to the phase drift. It could be, for instance, the AOM crystal, the RF transducer, or even the fiber coupling optics inside the AOM.

2.3 Mitigation method and results

As shown in the last section, the phase drift comes from the imbalanced heating between different f-AOMs. Therefore, we can mitigate this effect by heating up different f-AOMs equally. We can achieve this by applying a RF-signal at a frequency far detuned from the its center frequency. In that case, there is only a negligible amount of optical power going through while keeping the f-AOM heated to compensate the phase drift. In our case, we use the FiberQ series fiber attached AOM from G&H which has a 15.6 MHz 3 dB bandwidth[4]. We therefore choose the frequency of our compensation pulse at 100 MHz, which is far enough from the center frequency. Given the center frequency and the bandwidth of the f-AOM, we can estimate the optical power transmission at 100 MHz is suppressed by roughly 120 dB, which would lead to only an error of below 10^{-30} during a typical two-qubit gate. The schematic of our mitigation method is shown in Fig. 2.7.

We first run the 100 MHz compensation pulse at 100% power and tune the power of the test pulse, at 150MHz, to find the optimal compensation power. As shown in Fig. 2.8, we run the test pulse at different power to find the

[3]Here, we fit the first 50 points (roughly corresponding to first 10 seconds) in Fig. 2.6 (a), as there seems to be a saturation effect for longer time scale and the relative phase no longer drift at a constant speed.

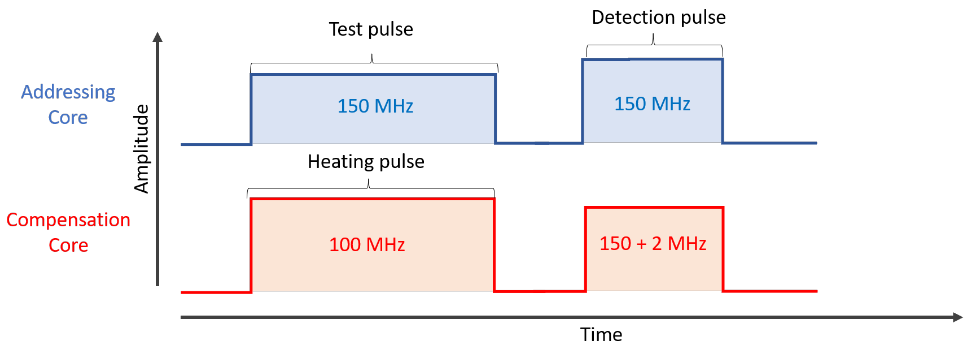

Figure 2.7: The schematic drawing of the mitigation method. A compensation pulse at 100MHz with higher amplitude is applied on the idle channels to balance the heating effect.

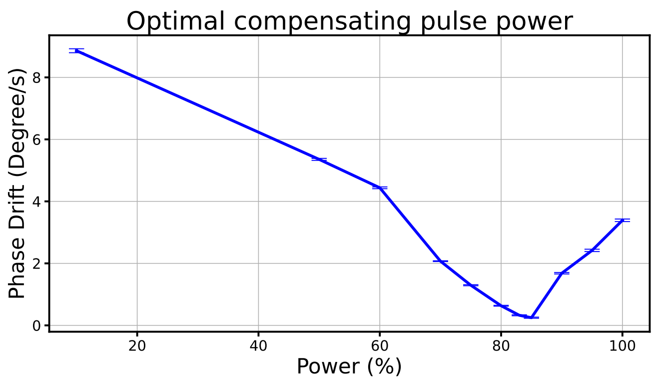

Figure 2.8: Find the optimal compensation power.

optimal value to mitigate the phase drift. The optimal value is found at around 83%. We further measure the RF absorption spectrum of the f-AOM, shown in Fig. 2.9, and find that the optimal compensation power we find matches the calculation result based on the RF absorption of the f-AOM very well.

In order to exclude the effect of detection pulse, we run the experiment with different test pulse lengths. Here, the detection pulse is set to be 100 μs long. As shown in Fig. 2.10, the test pulse dominant the effect when it is above 5 ms. There the phase drift is suppressed by an order of magnitude to around 2 degree per second.

After demonstrating the proof-of-principle experiment of the mitigation method. We further fine tune the power of the compensation pulse at different test pulse powers. The detailed curves similar to Fig. 2.8 can be seen in Appendix A. The results are summarized in Fig. 2.11 and Fig. 2.12. As shown in Fig. 2.11, the power ratio of the test pulse and the compensating pulse is

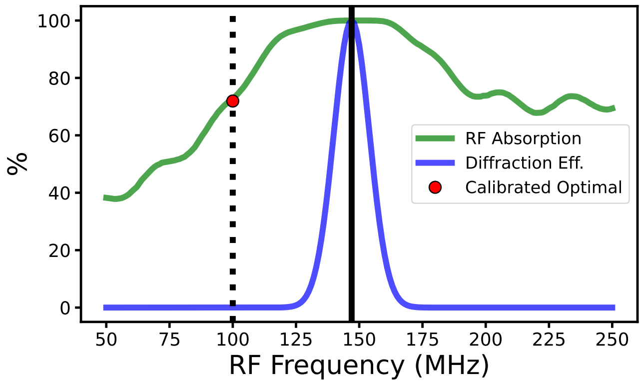

Figure 2.9: In this figure, the blue and green curves represent the optical transmission and RF absorption of the f-AOM. The optimal number of 83% corresponds to around 68% of actual power measured at the output of the DDS, which is shown as the red dot in the figure. This matches the measured RF absorption spectrum very well.

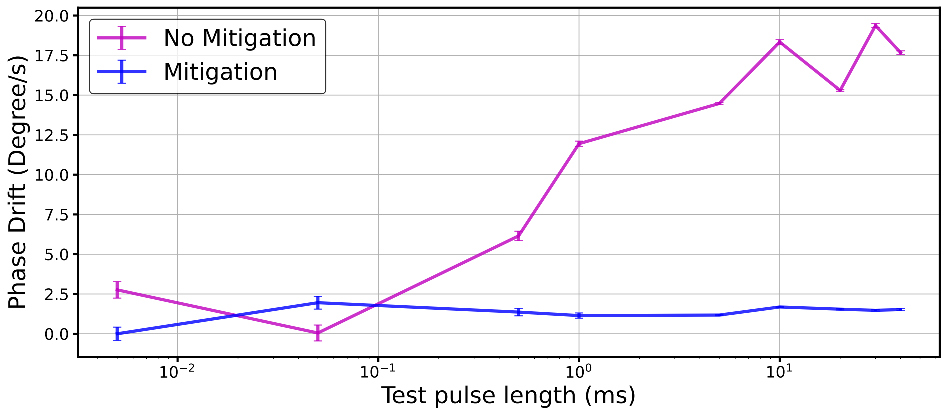

Figure 2.10: Comparing the phase drift with and without the compensation pulse at different pulse length.

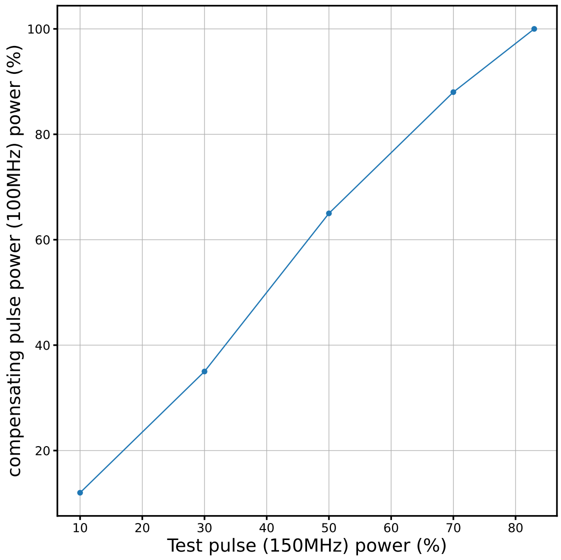

Figure 2.11: The optimal compensating pulse power while the test pulse is applied at different power levels.

nearly at constant. This implies that even without calibrating exhaustively at every power level, the phase drift can still be mitigated to an acceptable level by calculating the compensating power with this constant ratio.

The optimized phase drift result is shown in Fig. 2.12, where at all test pulse powers we used, the phase drift can be suppressed to below 1 degree per second. It is worth noticing that as we run the detection pulse at slightly different frequencies (2 MHz apart), the asymmetric heating effect caused by the detection pulse may also contribute to the phase drift. Therefore, in principle, we could further suppress the phase drift, if we can detect it directly with ions or simply increase the duty cycle of the test pulse during calibration. This phase drift can be corresponded to the errors while doing qubit operations. For instance, while doing coherent cross-talk compensation, approximately a 3° phase drift will lead to a 10^{-4} level cross-talk error. Therefore, suppressing the phase drift from around 20 degree per second to below 1 degree per second means we only need to re-calibrate the phase every few seconds rather than around 150ms.

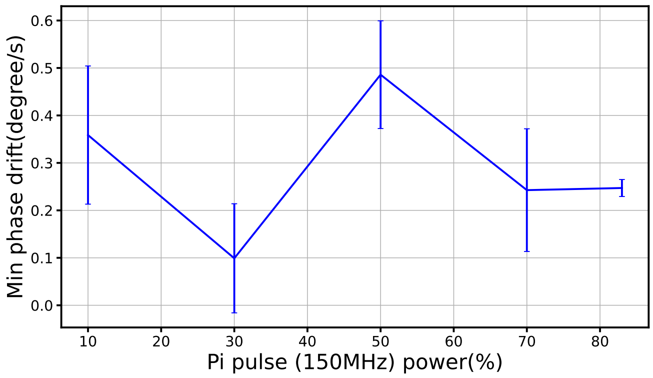

Figure 2.12: The mitigated relative phase drift between the two channels at different test pulse powers.

Chapter 3

Scalable addressing system

In the current setup, we have many output addressing channels with fixed input, i.e. beam splitted with fiber splitters. However, this means a waste of power when only some of the addressing channels are used. Therefore, as mentioned in section 1.2, we would like to design a selective addressing system. To switch between different target channels, it is necessary to be able to steer the beam around. This can be achieved by wavefront modulation device, such as Spatial light modulator (SLM) or digital micro-mirror device (DMD)[9] to form an arbitrary spatial pattern of the beam, or deflection devices, such as electric-optical deflector (EOD)[8], micro-electromechanical system (MEMS)[2, 1, 10], or acoustic optical deflector (AOD)[12]. In this thesis we will use on the AOD device to steer the beams thereby distributing powers between different addressing channels.

In section 3.1, we will discuss some of the beam deflection devices based on the three features we value, i.e. flexibility, speed and scalability, we mentioned in section 1.2. In section 3.2, the design of the AOD based system, which we decide to adapt in the LogiQ setup is discussed in detail.

3.1 Deflection devices

As discussed above, there are different ways to steer the beam around. A detailed comparison of these different methods has been conducted in Ref. [7]. As classified in Ref. [7], the beam steering device can be loosely classified into *mirror-based mechanical deflectors* and *optical solid state deflectors*. Generally speaking, the former is relatively slow but has a larger deflection range. The later, on the other hand, is usually faster but has a limited scanning range. This features are not strict. For instance, MEMS has been used as individual addressing systems for trapped-ions and cold atoms[2, 1, 10] with a switching speed at microseconds level. Large aperture AOD using acoustic mode with slow sound velocity or EOD based on materials like Potassium

Tantalate Niobate (KTN) with more significant Kerr effect[11] are also be able to address up to dozens or even hundreds of qubits. Although devices like MEMS, EOD and AOD can all be used to switch between different target qubits by steering the beam, the drawback of the former two is that they can not split the beam. Therefore, to address M qubits simultaneously, the laser beam has to be first split into M beams each controlled by a MEMS or EOD, thereby not as flexible as the AOD. Therefore, in this thesis we will design our selective addressing system based on AOD.

3.1.1 Acoustic optical deflector

The working principle of an acoustic optical deflector is similar to an AOM. The input RF signal is transferred to vibration by an piezoelectric transducer attached to a crystal. The vibrating transducer will then inject an acoustic wave to the crystal which leads to a periodic change of the index of refraction caused by expansion and compression of the crystal. Therefore, the injected light will experience a Bragg diffraction. Typically the light inject at the so-called Bragg angle,

$$\theta_B = \frac{\lambda F}{V},$$

where λ is the optical wavelength, F and V are the acoustic frequency and velocity respectively. At this injection angle the 1^{st} will have the largest power. The 1^{st} order deflected beam will then point at $-\theta_B$, forming a $\theta = 2\theta_B$ separation angle from the 0^{th} order injecting beam. However, unlike AOM, to achieve larger deflection angle some AOD would use an acoustic mode with much slower acoustic velocity.

The frequency, amplitude and phase of the optical beam can be easily controlled by an Acoustic Optical device. The frequency of the $+1^{st}$-order (-1^{st}-order) diffracted beam is up-shift (down-shift) by the acoustic frequency controlled by the applied RF signal. The amplitude and phase of the outgoing light can also be controlled by the amplitude and phase of the RF signal accordingly.

AOD is one of the most flexible device among all sorts of choices, as multiple RF signals at different frequencies can be applied to the device to generate multiple deflected beams. However, those generated beams are hence at slightly different frequencies. Therefore, to balance the frequency difference, frequency shifts are required for each of the generated beams downstream, which unavoidably increase the cost and complexity of the addressing system. However, this approach provides the benefit of fully individual controllability of all the channels. Another method to deal with the frequency difference is using a pair of crossed AODs. One can use the $+1^{st}$-order of the first one and the -1^{st}-order of the second to generate a sequence of beam spots without shifting the frequency. However, the drawback of this approach is that to generate M equal frequency spots M^2 spots have to be generated. Therefore, the efficiency of this method drops as $1/M$.

The speed of the AOD is determined by the rise time T_r, which is defined as the time interval for the light power to go from 10% to 90% of the maximum value. For a Gaussian beam, it is given by

$$T_r = 0.64\,\frac{D}{V}\,,$$

where D is the diameter of the laser beam. For a typical AOD using the shear mode of Tellurium Dioxide crystal whose acoustic velocity is around 670m/s. The rising time, T_r, for a 1mm diameter beam is slightly below 1¯s, which can be considered relative fast for trapped-ions system.

It seems that it is favorable to have focused beam injected into the AOD to achieve higher speed. However, there is a trade-off between the speed and the scalability of the system. Assuming the furthest two points we want to address is separated by a distance d, and each beam point is focused to a waist of the w at the final image plane. The ratio d/w is determined by the deflection angle separation of the two beams $\Delta\theta$ and the divergence half-angle of the Gaussian beam at the AOD, $\delta\theta$. We have

$$\frac{d}{w} = \frac{\Delta\theta}{\delta\theta} = \frac{\lambda\Delta F}{V}\frac{\pi w_0}{\lambda} = \frac{\pi D \Delta F}{2V} \approx 2.45\Delta F T_r, \tag{3.1}$$

where ΔF is limited by the bandwidth of the AOD, and w_0 is the beam width of the injecting beam. Here, we assume that the injected beam has minimum width at the center of the AOD crystal, thereby $w_0 = D/2$. Assuming a $10\mu m$ spacing and $1\mu m$ beam waist, more than 200 beam points can be generated without significant drop of efficiency using a large aperture wide-band AOD.

3.2 AOD based system

As discussed in the last section, we use an AOD to build our selective addressing system. In the setup, the 729nm beam will first go through a double-pass AOM to gain larger adjustable frequency range. Then, the beam will go through the multiplexing system and coupled to a laser-written waveguides array. Each waveguide will then be coupled to a single mode fiber and a fiber attached AOM which enables fully individual control. Finally, the fibers will again couple to a waveguide array, and the output beam will then be imaged to the ions. The schematic drawing of the addressing system is shown in Fig. 3.1. The laser beam coming from the Double-pass AOM is first adjusted to the right beam waist with a telescope and goes into the AOD. Deflected beams with different angles become parallel after the first

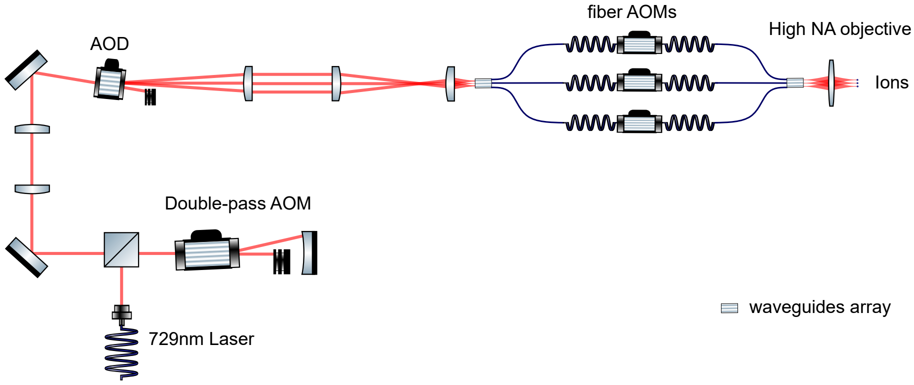

Figure 3.1: The schematic drawing of the addressing system. Here, we only draw three channels to illustrate the idea.

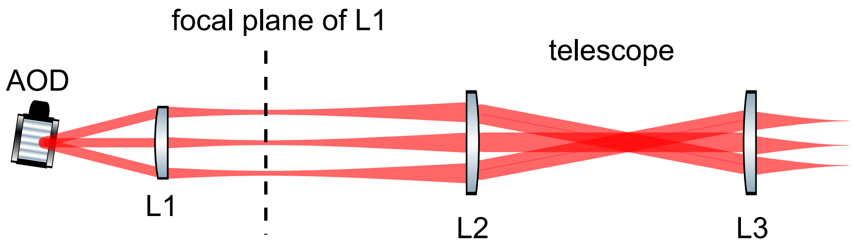

Figure 3.2: The schematic drawing of the optical system to match the deflected beams to the modes of the waveguides array.

lens and are focused at the focal plane of the first lens. Then, the beams are demagnified to match the mode size and spacing of the waveguides array by another telescope. In our case the mode size of the waveguides array is $2\,\mu m$ defined by the $1/e^2$ waist the Gaussian mode, and the spacing between adjacent waveguides is $15\,\mu m$. As discussed in last section, large aperture and wide bandwidth are favorable for the AOD. In the following thesis we will use the specified parameters of OAD1343-T70S-9 AOD from ISOMET for design purpose. The device has an active optical aperture of $9\,mm \times 9\,mm$. To avoid clipping effect of the aperture, we set the beam waist at the AOD to be $1.5\,mm$, i.e. $3\,mm$ in diameter. According to Eq.(3.1), the frequency difference between beams addressing two adjacent waveguides is around 1.06 MHz, given the sound velocity of 667 m/s according to the specification. The diffraction efficiency is promised to be larger than 80% in a 25 MHz to 30 MHz scanning range. Therefore, more than 20 channels can be addressed without significant loss of efficiency.

Table 3.1: Lenses we adapt for the AOD system

	item number	focal length	optic diameter	NA
L1	AL2550M-B	50 mm	25.0 mm	0.23
L2	AL50100M-B	100 mm	20.0 mm	0.23
L3	AL3026-B	26 mm	30.0 mm	0.52

As shown in the schematic drawing in Fig. 3.2, the first lens, L1, is placed a focal length away from the deflecting pivot of the AOD. The image on the focal plane of L1 is then demagnified to match the mode size of the waveguides array. Denoting the beam width at the AOD to be w_0, the beam width at the focal plane of the third lens L3, w is approximately given by

$$w \approx \frac{\lambda}{\pi w_0} \frac{f_1 f_3}{f_2}, \tag{3.2}$$

where f_2 and f_3 are the effective focal length of L2 and L3 respectively. Here, we assume $w_0 \gg \lambda$, e.i. the input beam to the AOD is collimated. The total length of the system from the deflection pivot of the AOD to the edge of the waveguides array is approximately $2(f_1 + f_2 + f_3)$. Based on Eq.(3.2), we choose the following lenses from Thorlab as listed in Tab. 3.1.

3.2.1 System efficiency estimation

As already mentioned in section 1.2, the individual addressing system can also be achieved by simply splitting the light into N channels, where N is the total number of qubits, and control each channels individually. In this section, we will compare the efficiency of these two systems and see the gain we can obtain by upgrading to the selective system.

If the AOD based selective system is not used, the output beam from the Double-pass AOM would be directly coupled to a single-mode fiber. Then the light will be split by fiber splitters, and each coupled to a f-AOM. Here, we assume that the coupling efficiency from free space to the single-mode fiber and the waveguides array are at similar level. Additionally, the loss in the fiber splitters is assumed to balance out the loss of light propagating in the waveguides and the coupling between the waveguides to the fibers. To make the comparison, we estimate the proportion of power for one of the channels to the total power in the splitting case. In the case of evenly splitting, there will be $1/N$ amount of power coupled to each of the channels, while in the multiplexing case it will be η/M, where M is the number of qubits we want to address simultaneously and η is the efficiency of the AOD and the additional free-space optics, i.e.

$$\eta = \eta_{fs}\eta_{AOD}\,. \tag{3.3}$$

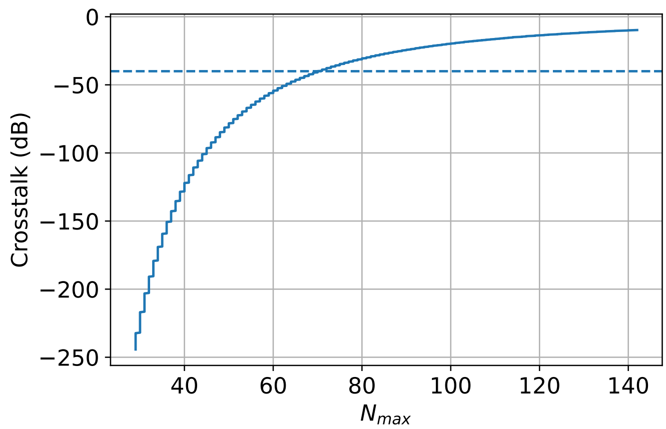

Figure 3.3: The relationship between crosstalk level and maximum number of reachable channels. The horizontal dashed line indicate the 10^{-4} level of crosstalk.

According to the specification of the AOD, we have $eta_{AOD} > 80\%$ over a range of at least 25 MHz. We further assume η_{fs} to be 95% which is a reasonable assumption for a few lenses and mirrors. Therefore, we have $\eta \approx 76\%$. Hence, the ratio of each channel's power for the selective system and the splitting system is given by,

$$\frac{P_{sel}}{P_{spl}} = \frac{\eta N}{M} \approx 0.76 \frac{N}{M} \tag{3.4}$$

3.2.2 Crosstalk and scalability

In principle, the spacing between neighboring waveguides can be reduced to increase the number of reachable channels within the band width of the AOD. However, this will also lead to larger crosstalk. The proportion of power coupled to the neighboring waveguides can be calculated by, $P = e^{-d^2/w_0^2}$. Assuming the AOD has a band width of 30MHz, the maximum distance the beam can travel at the edge of the waveguides is approximately $424\,\mu m$. Therefore the maximum number of reachable channels is $N_{max} = \lfloor 424/d \rfloor + 1$. As shown in Fig. 3.3, the system can be extend to about 70 channels while maintaining a crosstalk level of 10^{-4}.

Chapter 4

Conclusion

In this thesis, we focus on the individual laser addressing system of a trapped-ions system. We first investigate the relative phase stability between different channels and in the later half of the thesis, we design a more scalable addressing system by steering the beam around with an AOD.

We notice that the phase drift between different channels is mainly attributed to the heating effect of the f-AOM caused by the injected RF power. Based on this observation, we use a compensation pulse to heat up the idle f-AOMs equally at a far detuned frequency where the optical transmission is negligible. With this mitigation method, the phase drift can be stabilized to below 1 degree per second. This can potentially be further suppressed by fine tune the RF power of the compensation pulse.

In the later part of the thesis, we discuss the design of an AOD based system to selectively address M of N qubits. Details of the AOD device and relevant optical systems has been discussed. The selective system is estimated to be able to gain a factor of $0.76\frac{N}{M}$ of power comparing to simply splitting the power into all N channels. By re-design the waveguides array, the system can be extended to large systems at the cost of higher crosstalk. However, it is shown that as many as 70 channels can be addressed while keeping the crosstalk below 10^{-4} level.

Appendix A

Compensation pulse power tuning

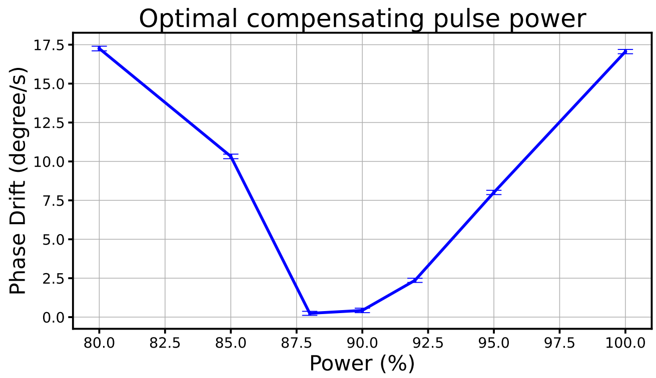

Figure A.1: Find the optimal compensation power while running the test pulse at 70% power.

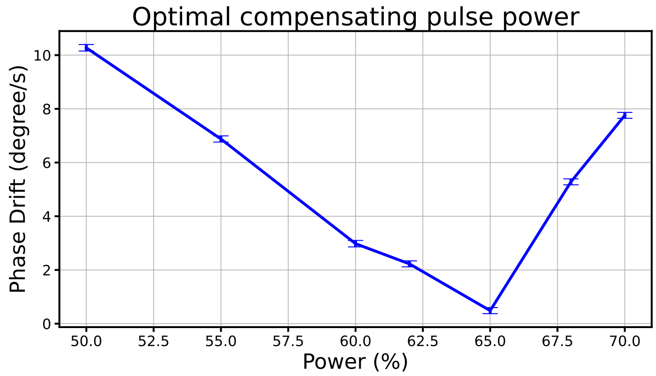

Figure A.2: Find the optimal compensation power while running the test pulse at 50% power.

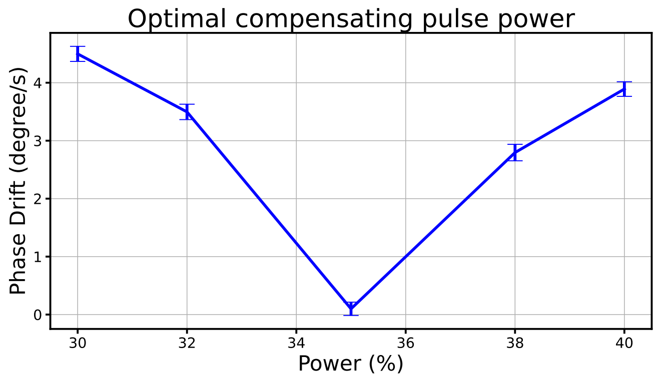

Figure A.3: Find the optimal compensation power while running the test pulse at 30% power.

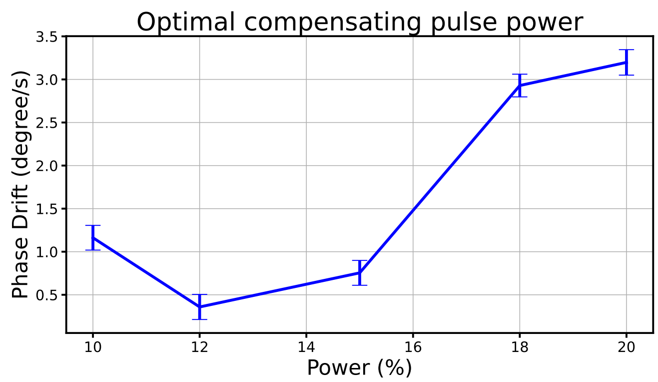

Figure A.4: Find the optimal compensation power while running the test pulse at 10% power.

Bibliography

[1] S Crain, E Mount, S Baek, and J Kim. Individual addressing of trapped 171yb+ ion qubits using a microelectromechanical systems-based beam steering system. *Appl. Phys. Lett.*, 105(18):181115, November 2014.

[2] Caleb Knoernschild, Changsoon Kim, Bin Liu, Felix P Lu, and Jungsang Kim. MEMS-based optical beam steering system for quantum information processing in two-dimensional atomic systems. *Opt. Lett.*, 33(3):273–275, February 2008.

[3] D Leibfried, R Blatt, C Monroe, and D Wineland. Quantum dynamics of single trapped ions. *Rev. Mod. Phys.*, 75(1):281–324, March 2003.

[4] Stefanie Miller. Optical pulse shaping for trapped-ion quantum computing with integrated photonics, 2019.

[5] Vlad Negnevitsky. Feedback-stabilised quantum states in a mixed-species ion system, 2018.

[6] Pedro Parrado-Rodríguez, Ciarán Ryan-Anderson, Alejandro Bermudez, and Markus Müller. Crosstalk Suppression for Fault-tolerant Quantum Error Correction with Trapped Ions. *Quantum*, 5:487, June 2021.

[7] G.R.B.E. Römer and P. Bechtold. Electro-optic and acousto-optic laser beam scanners. *Physics Procedia*, 56:29–39, 2014. 8th International Conference on Laser Assisted Net Shape Engineering LANE 2014.

[8] F Schmidt-Kaler, H Häffner, S Gulde, M Riebe, G P T Lancaster, T Deuschle, C Becher, W Hänsel, J Eschner, C F Roos, and R Blatt. How to realize a universal quantum gate with trapped ions. *Appl. Phys. B*, 77(8):789–796, December 2003.

[9] Chung-You Shih, Sainath Motlakunta, Nikhil Kotibhaskar, Manas Sajjan, Roland Hablützel, and Rajibul Islam. Reprogrammable and high-precision holographic optical addressing of trapped ions for scalable quantum control. *npj Quantum Information*, 7(1):1–8, April 2021.

[10] Ye Wang, Stephen Crain, Chao Fang, Bichen Zhang, Shilin Huang, Qiyao Liang, Pak Hong Leung, Kenneth R Brown, and Jungsang Kim. High-Fidelity Two-Qubit gates using a Microelectromechanical-System-Based beam steering system for individual qubit addressing. *Phys. Rev. Lett.*, 125(15):150505, October 2020.

[11] Yagi. KTN crystals open up new possibilities and applications. *NTT tech. rev.*, 2009.

[12] D D Yavuz, P B Kulatunga, E Urban, T A Johnson, N Proite, T Henage, T G Walker, and M Saffman. Fast ground state manipulation of neutral atoms in microscopic optical traps. *Phys. Rev. Lett.*, 96(6):063001, February 2006.

ETH

Eidgenössische Technische Hochschule Zürich
Swiss Federal Institute of Technology Zurich

Declaration of originality

The signed declaration of originality is a component of every semester paper, Bachelor's thesis, Master's thesis and any other degree paper undertaken during the course of studies, including the respective electronic versions.

Lecturers may also require a declaration of originality for other written papers compiled for their courses.

I hereby confirm that I am the sole author of the written work here enclosed and that I have compiled it in my own words. Parts excepted are corrections of form and content by the supervisor.

Title of work (in block letters):

Optical phase stabilization within a selective fiber network

Authored by (in block letters):
For papers written by groups the names of all authors are required.

Name(s):	**First name(s):**
Wang	Kaizhao

With my signature I confirm that
- I have committed none of the forms of plagiarism described in the 'Citation etiquette' information sheet.
- I have documented all methods, data and processes truthfully.
- I have not manipulated any data.
- I have mentioned all persons who were significant facilitators of the work.

I am aware that the work may be screened electronically for plagiarism.

Place, date

Zurich, 08/12/2022

Signature(s)

For papers written by groups the names of all authors are required. Their signatures collectively guarantee the entire content of the written paper.